Research in Astronomy and Astrophysics, 24:115017 (11pp), 2024 November https://doi.org/10.1088/1674-4527/ad86a8

A Novel Ephemeris Model for Martian Moons Incorporating Their Free Rotation

Yong-Zhang Yang[1], Kai Huang[1,2], Jian-Guo Yan[3], and Yu-Qiang Li[1]
[1] Yunnan Observatories, Chinese Academy of Sciences, Kunming 650216, China; yang.yongzhang@ynao.ac.cn, lyq@ynao.ac.cn
[2] University of Chinese Academy of Sciences, Beijing 100049, China
[3] State Key Laboratory of Information Engineering in Surveying, Mapping and Remote Sensing, Wuhan University, Wuhan 430070, China; jgyan@whu.edu.cn
Received 2024 May 13; revised 2024 September 27; accepted 2024 October 12; published 2024 November 12

Abstract

High-precision ephemerides not only support space missions, but can also be used to study the origin and future of celestial bodies. In this paper, a coupled orbit-rotation dynamics model that fully takes into account the rotation of the Martian moons is developed. Phobos and Deimos' rotations are first described by Eulerian rotational equations, and integrated simultaneously with the orbital motion equations. Orbital and orientational parameters of Mars satellites were simultaneously obtained by numerical integration for the first time. In order to compare the differences between our newly developed model and the one now used in the ephemerides, we first reproduced and simulated the current model using our own parameters, and then fit it to the Institut de Mécanique Céleste et de Calcul des Éphémérides ephemerides using least-square procedures. The adjustment test simulations show Phobos and Deimos' orbital differences between the refined model and the current model are no more than 300 m and 125 m, respectively. The orientation parameters are confirmed and the results are in good agreement with the International Astronomical Union results. Moreover, we simulated two perturbations (main asteroids and mutual torques) which were not included in our refined model, and find that their effects on the orbits are completely negligible. As for the effect on rotation, we propose to take care of the role of mutual attraction in future models.

Key words: planets and satellites: dynamical evolution and stability – methods: numerical – celestial mechanics – astrometry

1. Introduction

Mars is most similar to the Earth in the solar system and is the only terrestrial planet other than Earth to have natural satellites. Phobos and Deimos are the two moons of Mars. Since their discovery in 1877, the orbital motion of the Martian moons has been studied extensively. In order to fit the observation data to the study of the dynamical properties of the Martian moons: first Earth-based observations and then to spacecraft observations, a variety of dynamical models have been developed. During the Mariner and Viking era, Sinclair (1971, 1978) and Shor (1975) employed analytical expressions to fit various sets of Earth-based observations to generate the ephemerides and confirmed the secular tidal acceleration which was first studied by Sharpless (1945). Jacobson et al. (1989) and Sinclair (1989) used all available positional observations of satellites of Mars, including Earth-based and from the Mariner 9 and Viking spacecraft, to re-determine the orbits of the Martian moons, and these ephemerides are available in the SPICE (Arora & Russell 2010) library until now.

The first completely numerical dynamical model of Martian moons was studied by Lainey et al. (2007) during the Mars Express (MEX) mission; the model presented in this work used: (1) the aspherical Martian gravity field, (2) the perturbations of the Sun, Jupiter, Saturn, the Earth, and the Moon using planetary ephemerides, (3) the IAU2000 Martian precession/rotation, (4) the mass of each Martian moon, and the tidal effect was modeled by the tidal bulge raised by each moon on Mars using physical formulation instead of fitting secular accelerations in the satellite longitudes. After fitting to the MEX, Mars Global Surveyor (MGS), Phobos 2, Viking 1–2, Mariner 9, and ground based observations, new ephemerides of the Martian moons have been developed on the basis of the first numerical dynamical model. It is worth mentioning that, although the authors realize that the perturbations due to the librations of the Martian moons have a significant influence that cannot be ignored, this effect was not modeled due to the lack of an accurate C_{20} and estimated libration angles (Lainey et al. 2007).

Jacobson (2010) upgraded the dynamical model of the Martian satellites, introducing the effect of Phobos' libration in the form of an analytical formula for the first time. Assuming Phobos is rotating synchronously, its pole is perpendicular to the orbital plane, and its axis of minimum principal moment of inertia points toward Mars. The angle between Phobos' axis of minimum principal moment of inertia and the direction from Phobos to Mars, also called libration angle, is small and can be

described by

$$\theta = (2e + \mathcal{A})\sin M, \tag{1}$$

where $\mathcal{A}$ is the libration amplitude and can be calculated from the moment of inertia (Chao & Rubincam 1989), and e and M are Phobos' orbital eccentricity and mean anomaly in its orbit, respectively. The revised orbits of Martian moons were obtained by fitting the numerical dynamical model to all available Earth-based observations, imaging observations and radio tracking data from spacecraft.

The above dynamical model has been used until now, and although observational data have been accumulating over time, the dynamical model has introduced only minor additions. Examples include (1) mutual attraction between satellites, (2) general relativity, and (3) the second gravitational field of satellites (Jacobson & Lainey 2014; Lainey et al. 2020). This is mainly due to the difficulty of determining the gravitational coefficients of Phobos and Deimos with current observations.

The Martian Moons eXploration (MMX) mission is under development by the Japan Aerospace Exploration Agency (JAXA), and is scheduled to be launched in 2026. This mission is dedicated to survey the two Martian moons and return samples from Phobos (Kawakatsu et al. 2023). In order to achieve the objective of collecting samples from Phobos, a probe will land on the surface of Phobos. At that time, there will be tracking data between the lander and the Earth, and these new data will offer new opportunities to study the orbital and rotational motions of the Martian moons.

Inspired by the MMX mission, this paper presents a refined numerical dynamical model for libration of the Martian moons. The libration is described using the Euler-Liouville equations, i.e., with a state of complete free rotation that does not take into account any assumptions. This dynamical model will allow us to study the motions of the Martian moons in the future with more realistic scenarios based on new observational data, such as the ones from MMX. In Section 2 we briefly introduce the dynamical model now in use. In Section 3 we detail our optimized libration model of the Martian moons. Section 4 provides a detailed comparison of these two models, followed by Section 5 where we summarize and conclude the paper.

2. Review of Numerical Dynamical Model

In this work, we will apply the numerical model now in use as a reference to study its differences with our revised model. Hence, we first introduce the modeling process of an ephemeris model.

The equations of translational motion are described in a planetocentric (Mars) reference system with fixed axes that align with the International Celestial Reference System (ICRS). The position vectors of the eight planets and the Sun relative to Mars in this reference system can be easily retrieved from the numerical ephemerides. Here we use the latest version of the planetary ephemeris INPOP21a provided by Institut de Mécanique Céleste et de Calcul des Éphémérides (IMCCE) to obtain the position and velocity vectors of the Sun and planets relative to Mars in the Barycentric Celestial Reference System (BCRS; Fienga et al. 2021). This ephemeris updates the Mars orbit relative to INPOP19a (Fienga et al. 2020), adding an additional 2 yr of data from MEX.

The orbital motion of the satellites around Mars can be described in terms of position $\boldsymbol{r} \equiv (r_x,\ r_y,\ r_z)$ and velocity $\boldsymbol{v} \equiv (v_x,\ v_y,\ v_z)$ in rectangular coordinates. The classical differential equations of relative motion in the planetocentric system can be read as,

$$\frac{d^2\boldsymbol{r}}{dt^2} = \frac{\boldsymbol{F}_s}{m_s} - \frac{\boldsymbol{F}_0}{m_0}, \tag{2}$$

where $\boldsymbol{F}_s$ and $\boldsymbol{F}_0$ indicate all the external forces exerted on the satellites and Mars, m_s is the mass of the satellite, m_0 is the mass of Mars, and t is the time expressed in the Barycentric Dynamical Time (TDB) timescale.

The forces that induce the relative motion can be split up into a two-body part, a part for third-body perturbation, a part for mutual attraction, a part for tidal perturbation, a part for relativistic perturbation and a part for spin librations. Hence, the $\frac{d^2\boldsymbol{r}}{dt^2}$ can be rewritten as:

$$\begin{aligned}\frac{d^2\boldsymbol{r}}{dt^2} &= \boldsymbol{a}_{\mathrm{two-body}} + \boldsymbol{a}_{\mathrm{third-body}} \\ &\quad + \boldsymbol{a}_{\mathrm{mutual}} + \boldsymbol{a}_{\mathrm{tide}} + \boldsymbol{a}_{\mathrm{rel}} + \boldsymbol{a}_{\mathrm{libr}}.\end{aligned} \tag{3}$$

Here the $\boldsymbol{a}_{\mathrm{two-body}}$, $\boldsymbol{a}_{\mathrm{third-body}}$ and $\boldsymbol{a}_{\mathrm{rel}}$ have the usual form used in numerical ephemerides (Folkner et al. 2014; Pitjeva & Pavlov 2017; Viswanathan et al. 2017).

If we consider Deimos as a third body, we can calculate the effect of Deimos on Phobos' orbit. According to the third-body perturbation equation, the acceleration of Phobos due to mutual attraction can be described as

$$\boldsymbol{a}_{\mathrm{mutual,p}} = \mu_{\mathrm{d}}\left(\frac{\boldsymbol{r_d} - \boldsymbol{r_p}}{r_{\mathrm{pd}}^3} - \frac{\boldsymbol{r_d}}{r_{\mathrm{d}}^3}\right). \tag{4}$$

Similarly, the acceleration of Deimos due to mutual attraction is

$$\boldsymbol{a}_{\mathrm{mutual,d}} = \mu_{\mathrm{p}}\left(\frac{\boldsymbol{r_p} - \boldsymbol{r_d}}{r_{\mathrm{dp}}^3} - \frac{\boldsymbol{r_p}}{r_{\mathrm{p}}^3}\right). \tag{5}$$

Here μ_d, μ_p, $\boldsymbol{r_d}$ and $\boldsymbol{r_p}$ are the product of the gravitational constant and the masses of Deimos and Phobos, and the position vectors of Deimos and Phobos relative to Mars in the inertial system, respectively. r_{p} denotes the norm of $\boldsymbol{r_p}$, r_{d} signifies the norm of $\boldsymbol{r_d}$, and $\mathrm{r_{dp}} = \mathrm{r_{pd}} = |\boldsymbol{r_p} - \boldsymbol{r_d}|$.

For tidal acceleration $\boldsymbol{a}_{\mathrm{tide}}$, Lainey et al. (2007) and Jacobson (2010) employed a different but similar form of model in their numerical integration. In this paper, we simulate the differences

between our new model and the French Numerical Orbit and Ephemerides (NOE), hence, here we refer to Lainey et al. (2007) for a complete description of the tidal force $\boldsymbol{F}_T$ acting on the satellite of the form

$$\boldsymbol{F}_T = -\frac{3k_2\mu_s m_s a_m^5}{r^8}\left(\boldsymbol{r} + \Delta t\left[\frac{2\boldsymbol{r}(\boldsymbol{r}\cdot\boldsymbol{v})}{\mathrm{r}^2} + (\boldsymbol{r}\times\boldsymbol{\Omega} + \boldsymbol{v})\right]\right), \tag{6}$$

where:

k_2 = the Love number of Mars
$\boldsymbol{\Omega}$ = the Martian angular velocity vector
$\mu_s = GM$ of Satellite
m_s = mass of Satellite
Δt = the time delay due to viscoelastic response of Mars
a_m = the equatorial radius of Mars.

Finally, we present the satellites' figure acceleration and libration model used in the current ephemerides of Martian moons. Under the assumption that the spin pole is normal to the orbital plane, according to Equation (1), the quadrupole force on Mars exerted by a satellite can be computed as

$$\boldsymbol{F}_m = \frac{3}{2}\mu_s\left(\frac{{a_m}^2}{r^4}\right)[(-C_{20} + 6C_{22}\cos 2\theta)\,\hat{\boldsymbol{r}} + 4C_{22}\sin 2\theta\,\hat{\boldsymbol{t}}], \tag{7}$$

where C_{20} and C_{22} are the second zonal and sectorial harmonic of the satellite respectively, $\hat{\boldsymbol{r}}$ denotes the unit vector directed from Mars toward the satellite and $\hat{\mathbf{t}}$ signifies the unit vector in the satellite's orbit plane normal to $\hat{\boldsymbol{r}}$ and in the direction of its orbital motion. Therefore, the reaction force acting on the satellite is

$$\boldsymbol{F}_s = -\left(\frac{\mu_m}{\mu_s}\right)\boldsymbol{F}_m, \tag{8}$$

with μ_m denoting the GM of Mars.

Utilizing Equations (4)–(8) to calculate $\boldsymbol{a}_{\mathrm{mutual}}$, $\boldsymbol{a}_{\mathrm{tide}}$, and $\boldsymbol{a}_{\mathrm{libr}}$ in turn and summing them up together with $\boldsymbol{a}_{\mathrm{two-body}}$, $\boldsymbol{a}_{\mathrm{third-body}}$ and $\boldsymbol{a}_{\mathrm{rel}}$, we then have the orbital equations of motion in the planetocentric coordinates.

3. Rotation Model of the Martian Moons

In this paper, the Martian moons are modeled as rigid bodies as in our previous study of Phobos' libration (Yang et al. 2020). The orientations of Phobos and Deimos are integrated from the differential equations for their angular velocities. The angular momentum vector of a satellite is the product of angular velocity and moment of inertia. The angular momentum vector varies with time due to external torques.

The process of modeling rotation is presented here using Phobos as an example. In order to describe the variations of Phobos' rotation in the inertial frame, for convenience, the frame of Phobos was aligned with its principal axis (PA). Then the orientation of Phobos' frame with respect to (w.r.t.) the inertial frame is determined by three Euler angles: ϕ, θ, and ψ, which vary with time t. The transformation from the inertial system to the body-fixed system (PA) is given by the matrix

$$R_{B2C} = R_z(\phi(t))R_x(\theta(t))R_z(\psi(t)), \tag{9}$$

where the rotation matrices R_z and R_x are right-handed rotations around the z-axis and x-axis, respectively. Hereafter, for simplicity, the argument t will be omitted where appropriate.

In a rotating system, the rate of change of angular velocity $\boldsymbol{\omega}$ is related to the torque $\boldsymbol{T}$ and determined by Euler-Liouville's equations of rotation,

$$\frac{d}{dt}(\boldsymbol{I}\boldsymbol{\omega}) + \boldsymbol{\omega}\times\boldsymbol{I}\boldsymbol{\omega} = \boldsymbol{T}, \tag{10}$$

where $\boldsymbol{I}$ represents the moment of inertia tensor. This leads to the equations for $\boldsymbol{\omega}$, consequently,

$$\frac{d\boldsymbol{\omega}}{dt} = \boldsymbol{I}^{-1}\left(\boldsymbol{T} - \frac{d\boldsymbol{I}}{dt}\boldsymbol{\omega} - \boldsymbol{\omega}\times\boldsymbol{I}\boldsymbol{\omega}\right). \tag{11}$$

The effect of elastic deformation is not considered in the current modeling because its effect on the Phobos ephemeris is less than 100 m even if Phobos k_2 is as large as 1×10^{-4} (Yang et al. 2024), corresponding to an extremely porous Phobos (Le Maistre et al. 2013), which we consider unlikely, since the porosity of Phobos is limited by the density of the material that makes the matrix of the bulk material. Hence, $\boldsymbol{I}$ is diagonal and constant. Solving Equation (11) for $\frac{d\boldsymbol{\omega}}{dt}$ we find that the resultant angular acceleration takes a simple form

$$\frac{d\boldsymbol{\omega}}{dt} = \boldsymbol{I}^{-1}(\boldsymbol{T} - \boldsymbol{\omega}\times\boldsymbol{I}\boldsymbol{\omega}). \tag{12}$$

The components of the angular velocity vector in the body-fixed system are easily expressed in terms of reference Euler angles (ϕ, θ, ψ) (Goldstein et al. 2002):

$$\begin{aligned}\omega_1 &= \dot\theta\cos\psi + \dot\phi\sin\psi\sin\theta\\ \omega_2 &= -\dot\theta\sin\psi + \dot\phi\cos\psi\sin\theta\\ \omega_3 &= \dot\phi\cos\theta + \dot\psi,\end{aligned} \tag{13}$$

where (ϕ, θ, ψ) are the precession angle, nutation angle, and rotation angle, respectively.

If we differentiate Equations (13) w.r.t. time t and rearrange them, we get a linear system of equations containing $\ddot\phi$, $\ddot\theta$ and $\ddot\psi$,

$$\begin{aligned}\ddot\phi &= \csc\theta(\dot\omega_1\sin\psi + \dot\omega_2\cos\psi + \dot\theta\dot\phi) - \dot\psi\dot\theta\cot\theta\\ \ddot\theta &= \dot\omega_1\cos\psi - \dot\omega_2\sin\psi - \dot\phi\dot\psi\sin\theta\\ \ddot\psi &= \dot\omega_3 - \ddot\phi\cos\theta + \dot\psi\dot\theta\sin\theta.\end{aligned} \tag{14}$$

The above equations model the Euler angle equations of motion, and the key is to calculate the angular acceleration $\frac{d\boldsymbol{\omega}}{dt}$, which can be evaluated by Equations (10)–(12). Having

Table 1
Parameters used in the Dynamical Model

Parameters	Value	Notes	Reference
The Sun and planets	⋯	INPOP21a	Fienga et al. (2021)
Gravity field of Mars	⋯	MRO120F, up to degree 12	Konopliv et al. (2020)
Martian precession/rotation	⋯	Quoted from MRO120F	Konopliv et al. (2020)
$k_{2,M}$	0.169	Martian Love number	Konopliv et al. (2020)
Q_M	99.5	Martian dissipation factor	Jacobson & Lainey (2014)
$\delta\bar{J}_{3,M}$	⋯	Seasonal gravity change of Mars	Konopliv et al. (2006, 2011, 2020)
Gravity field of Phobos	⋯	Forward model, up to degree 2	Yang et al. (2020)
$\mathcal{R}_P$	10.993	Radius, km	Willner et al. (2014)
GM_P	0.7072×10^{-3}	GM of Phobos	Pätzold et al. (2014)
Moment of inertia of Phobos	0.35545, 0.41811, 0.49134	Normalized by MR^2	Yang et al. (2020)
Gravity field of Deimos	⋯	Forward model, up to degree 2	Rubincam et al. (1995)
$\mathcal{R}_D$	6.25	Radius, km	Rubincam et al. (1995)
GM_D	0.98×10^{-4}	GM of Deimos	Konopliv et al. (2006)
Moment of inertia of Deimos	0.338, 0.461, 0.508	Normalized by MR^2	Rubincam et al. (1995)

established the mathematical equation for the Euler angle and external torques through angular acceleration, we now derive the calculation of external torques.

The calculation of the torque $\boldsymbol{T}$ applied to a satellite is usually divided into two parts: a torque from point mass (body) A to the satellite's figure and a torque from the oblateness (J_2) of Mars to the satellite's figure,

$$\boldsymbol{T} = \boldsymbol{T}_{\rm pm} + \boldsymbol{T}_{\rm fig}. \tag{15}$$

A detailed description of $\boldsymbol{T}$ and $\boldsymbol{I}$ can be found in Williams et al. (2001), Rambaux et al. (2012), Folkner et al. (2014), Pavlov et al. (2016) and Yang et al. (2020).

The instantaneous state of rotation of a rigid body can be defined completely by the six quantities, i.e., the above-defined Euler angles and their rates of change. In this paper, we use the above approach to model the libration of Phobos and Deimos, unlike the models used in the present ephemerides (pole normal to its orbit plane), the Martian moons are completely free to rotate without any assumptions.

4. Comparison

The studies of the rotation and orbital motion of the Martian moons described in the previous sections are motivated by the high-precision observational data that may be available from future missions, such as a probe's orbital data and satellite image data when the probe is at a very close distance. In addition, in particular, lander tracking measurements were carried out on Phobos (Kawakatsu et al. 2017; Usui et al. 2018). In this section, we simulate our new dynamical model incorporating the free rotation of the Martian moons, and then compare and analyze our model w.r.t. the current ephemeris models.

4.1. Methodology

In our numerical model, there are a number of parameters whose values affect the orbit significantly, such as the Martian gravitational field, and the satellite's initial position and velocity. In order to clarify the differences between the fully coupled approach and the simple libration model (i.e., Equations (7)–(8)) used so far, we borrowed from previous approaches (Yang et al. 2024) and first simulated the current simple model (Lainey et al. 2007, 2020; Jacobson 2010; Jacobson & Lainey 2014), but with our own selected physical parameters listed in Table 1. We then fitted the twelve initial parameters (positions and velocities of Phobos and Deimos) as our solve-for parameters to fit the current ephemeris. This fit resolves the issue of differing parameters and provides the best reference to investigate the differences between the new full model and the ephemeris model used so far. To fit the parameters of the model, we introduce this common relational formula,

$$\frac{\partial}{\partial P_j}\left(\frac{d^2\boldsymbol{r}_i}{dt^2}\right) = \frac{1}{m_i}\left[\sum_k\left(\frac{\partial \boldsymbol{F}_k}{\partial \boldsymbol{r}_k}\frac{\partial \boldsymbol{r}_k}{\partial P_j} + \frac{\partial \boldsymbol{F}_k}{\partial \dot{\boldsymbol{r}}_k}\frac{\partial \dot{\boldsymbol{r}}_k}{\partial P_j} + \frac{\partial \boldsymbol{F}_k}{\partial \Phi_k}\frac{\partial \Phi_k}{\partial P_j} + \frac{\partial \boldsymbol{F}_k}{\partial \dot{\Phi}_k}\frac{\partial \dot{\Phi}_k}{\partial P_j} + \frac{\partial \boldsymbol{F}_k}{\partial P_j}\right)\right], \tag{16}$$

where Φ and $\dot{\Phi}$ are the Euler angles and their rates, respectively. In particular, Φ and $\dot{\Phi}$ are not modeled in the ephemeris model and should be omitted. P_j denotes the unspecified parameter of the model that shall be fit (such as initial positions, velocities, Euler angles, etc.), then the variational equations are integrated simultaneously with the dynamical model.

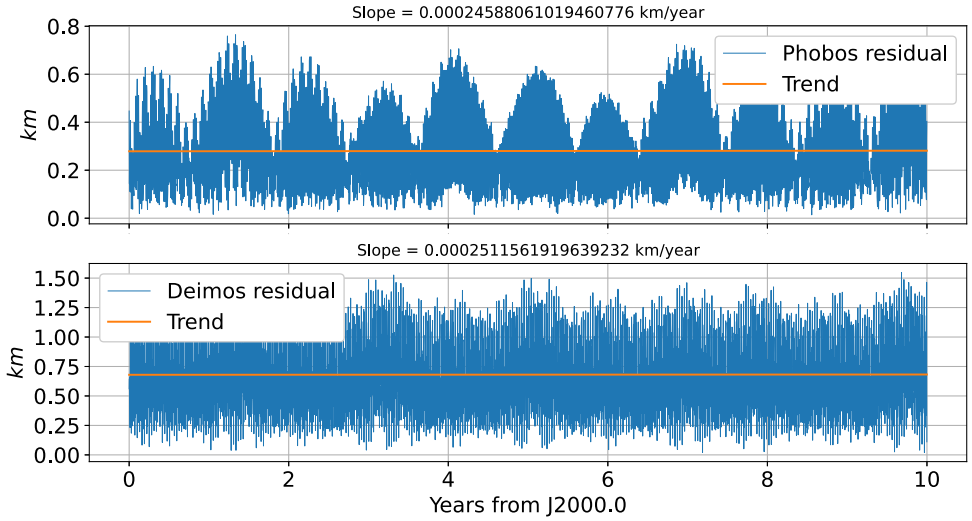

Figure 1. Differences in position after fitting the numerical model to the NOE ephemerides for Phobos (upper panel) and Deimos (lower panel). The satellites' initial positions and velocities have been determined.

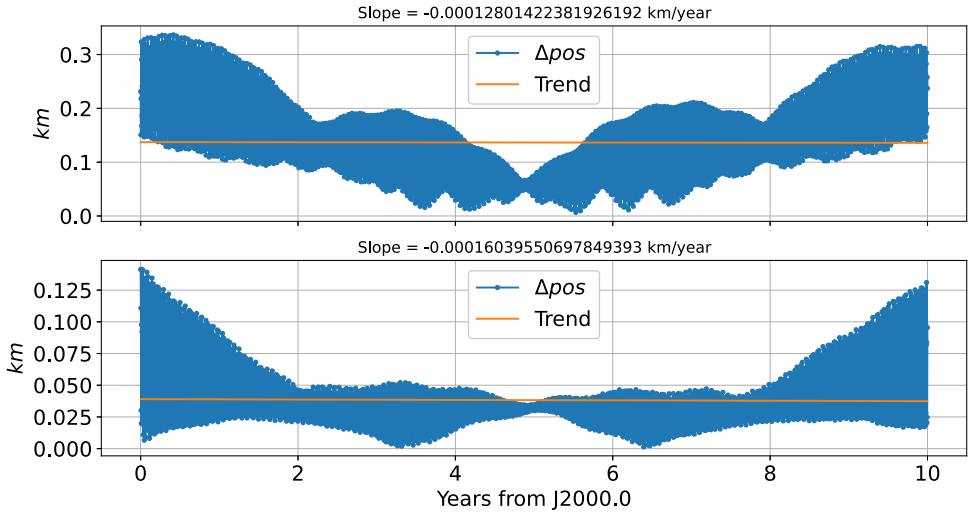

Figure 2. Difference in distances after 10 yr fitting between our refined model to the simulated simple model, Phobos (upper panel) and Deimos (lower panel). The satellites' initial positions, velocities, Euler angles and their rates have been determined here.

4.2. Fit to NOE Ephemerides

We chose the latest Martian ephemerides NOE-4-2020 (Lainey et al. 2020) as the "observational data" and fit our simple model to them. The adjustment was performed by least-squares in Cartesian planetocentric coordinates J2000, using a sample set of 3650 points with a step size of one day (ten years), with no weights assigned. We started with the initial epoch at JD 2451545.0 (J2000.0, TDB timescale) and we integrated the model over a decade. The residuals after fit are shown in Figure 1. The resulting differences in the positions are probably explained by the different physical parameters (such as the physical libration $\mathcal{A}$, the C_{20} and C_{22} of the satellites, the Martian dissipation factor Q, etc.) in these two models.

4.3. Fit to the Ephemeris Model

In order to explore the differences between our refined new dynamical model and the previous ephemeris model (Jacobson 2010; Jacobson & Lainey 2014; Lainey et al. 2020), we adjusted our new refined model to the simulated ephemeris integrated in Section 4.2, with the parameters of these two physical models being identical, so the differences are mainly due to the fact that the details of the models are not identical.

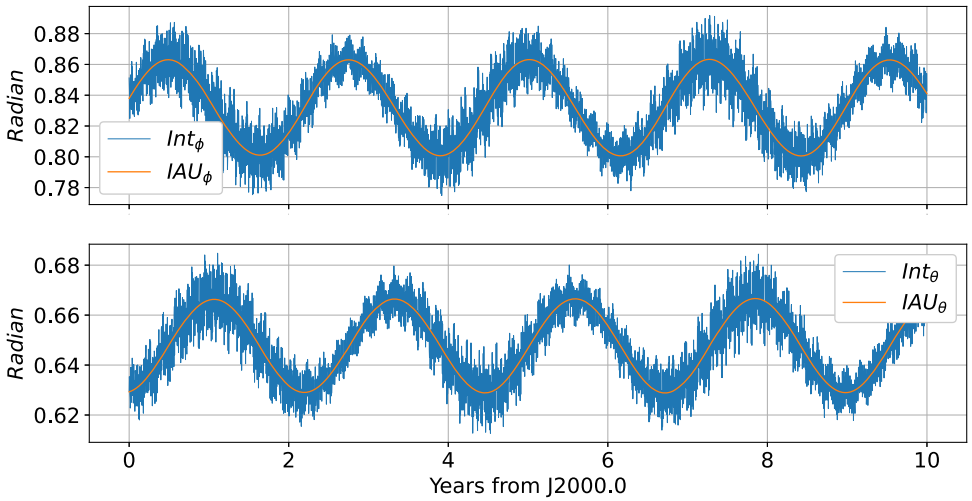

Figure 3. Temporal evolution of Phobos' precession angle ϕ and nutation angle θ over ten years. Here the numerical integration results are shown in blue and the IAU results are shown in red.

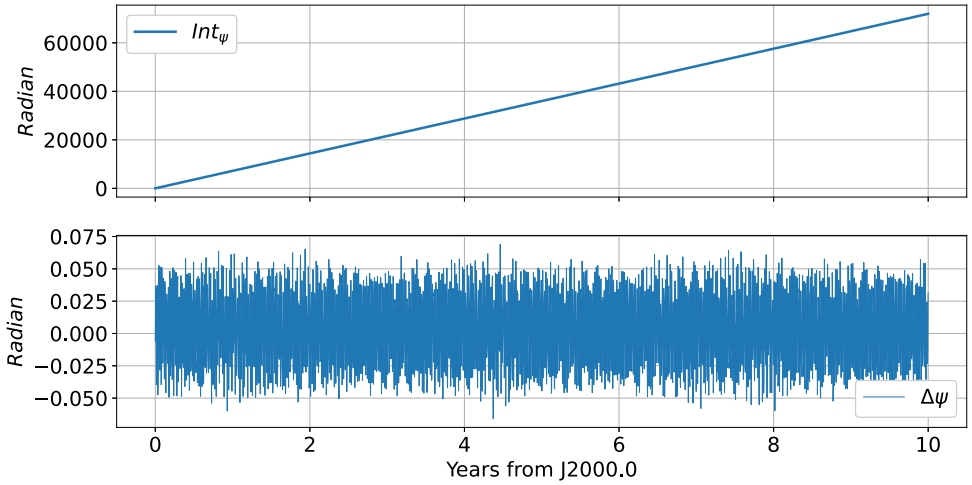

Figure 4. Temporal evolution of Phobos' rotation angle ψ (upper panel) and its difference compared to IAU's model (lower panel) over 10 yr.

We select the twenty-four initial conditions (each satellite's position, velocity, Euler angles and their rates) as our solve-for parameters to fit the simulated result in the previous section. The initial Euler angles and rates are referred from the International Astronomical Union (IAU) rotational elements (Archinal et al. 2018). Then the least-square procedures are applied to the model. Figure 2 shows the differences in distance after adjustment. The positional deviation may be due to the newly introduced Phobos latitudinal libration and the different longitudinal librations in the refined model.

One of the advantages of our refined model is that the Euler angles of the Martian moons and their rates can be obtained by numerical integration. Here the evolutions of the Euler angles defined w.r.t. the inertial reference frame for 10 yr from 2000 to 2010 January 1 (TDB timescale) are plotted in Figures 3–6. Phobos and Deimos' precession angle ϕ and nutation angle θ are plotted along with IAU's modeling results in Figures 3 and 5, respectively. The rotation angles ψ obtained by integration and their difference from the IAU's result are shown in Figures 4 and 6, respectively. Although the reference frame used by IAU is slightly different from the one we used (Archinal et al. 2018), the results are still in pretty good agreement. To characterize the high-frequency spectrum of the difference between our numerical integration results and the IAU polynomials, we decomposed the difference in frequency domain by employing the method used in Yang et al. (2017, 2019). The period and frequency of the largest amplitude term is shown in Table 2. These high-frequency

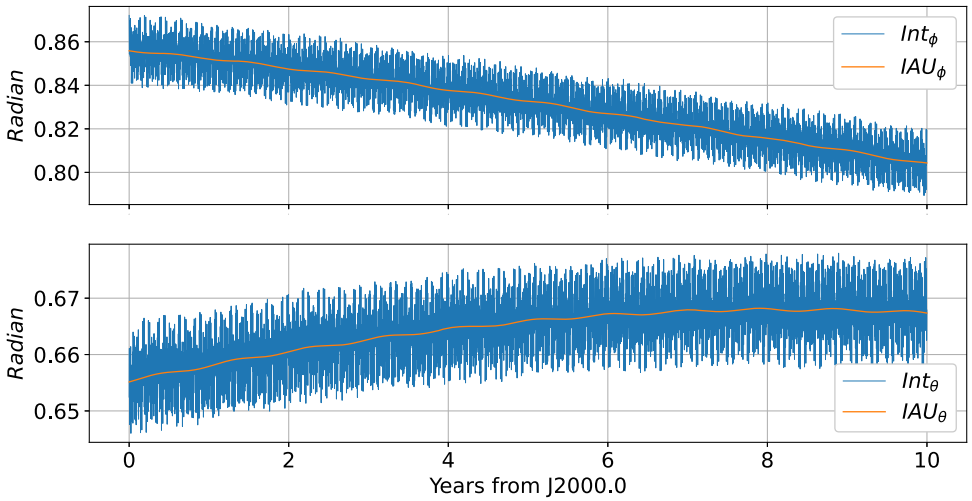

Figure 5. Temporal evolution of Deimos' precession angle ϕ and nutation angle θ over ten years. The numerical integration results are shown in blue and the IAU models are shown in red.

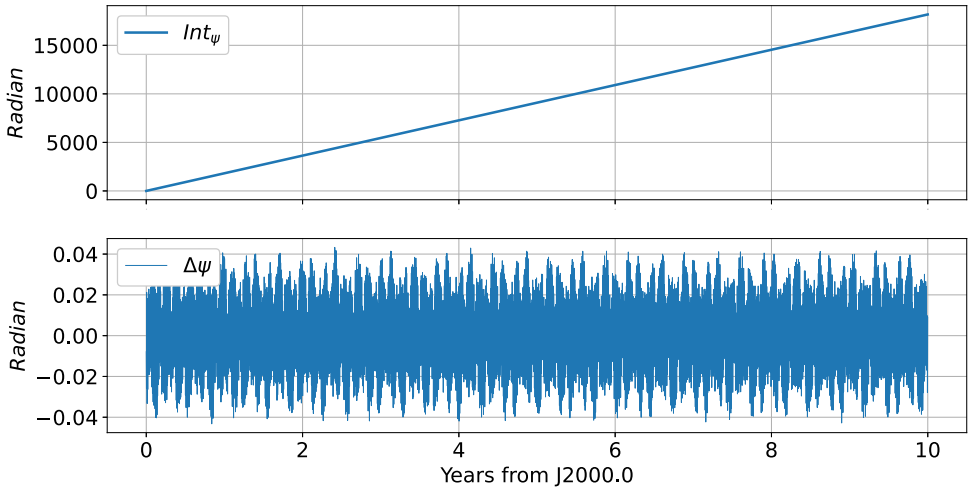

Figure 6. Temporal evolution of Deimos' rotation angle ψ (upper panel) and its difference compared to IAU's result (lower panel) over 10 yr.

oscillations are due to the rotational motion of the satellites and their orbital motion around Mars.

To demonstrate the difference between the libration of the two models, Figure 7 presents the longitude of the direction from Martian moons to Mars and the moons' axis of minimum principal moment of inertia w.r.t. the two models. By comparison, we can see that the differences between the two dynamical models are very small, indicating that the deviation in the longitude direction can be described by the simple model well (Equation (1)). The moons' obliquities are shown in Figure 8. Based on the assumption that the pole is normal to the orbital plane, these parameters were not considered in the

Table 2
Frequency Analysis of the Difference Between Numerical Integration Results and the IAU Polynomials

Satellite	Arg	Per (days)	Fre (rad day^{-1})	Amp (rad)
Phobos	$\Delta\phi$	0.2333	26.9325	0.0082
	$\Delta\theta$	0.2333	26.9325	0.0049
	$\Delta\psi$	0.3190	19.6944	0.0311
Deimos	$\Delta\phi$	0.9596	6.5480	0.0061
	$\Delta\theta$	0.9596	6.5480	0.0040
	$\Delta\psi$	1.2625	4.9768	0.0281

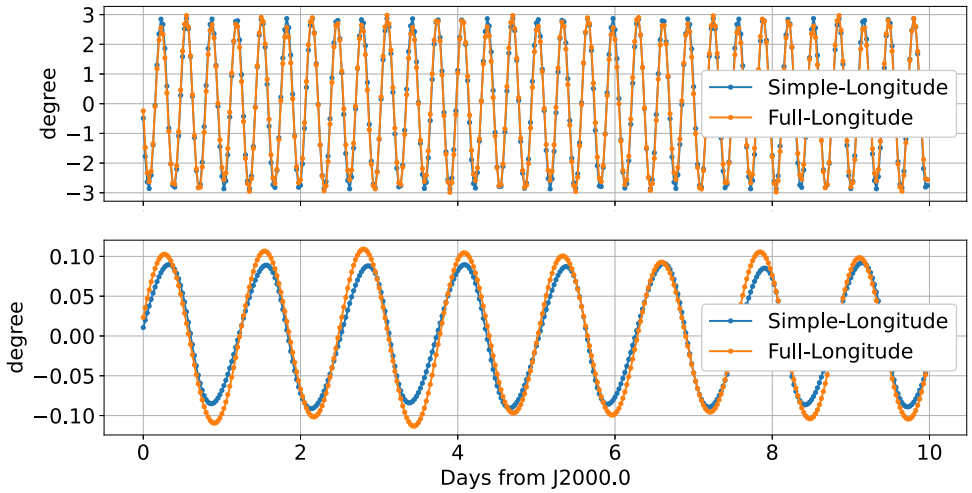

Figure 7. Longitude of Mars in the Martian moons' principal axis coordinate system, upper panel for Phobos, lower panel for Deimos.

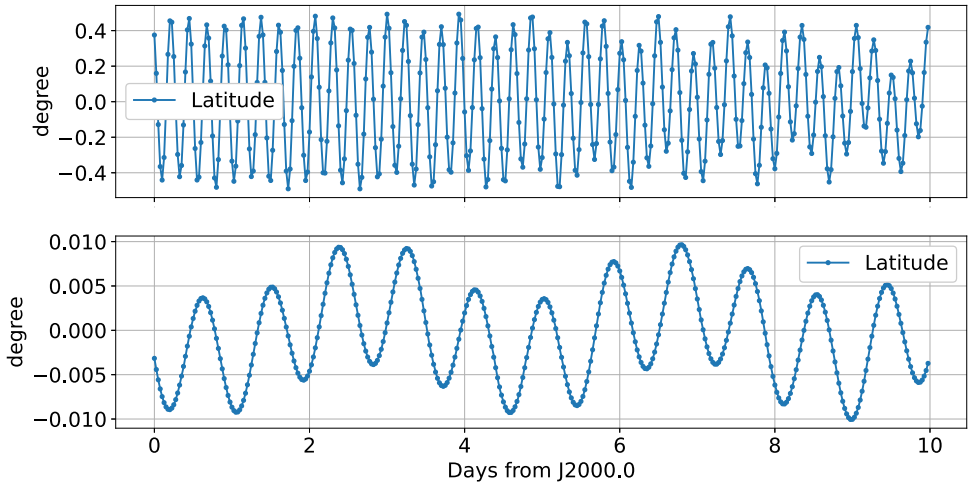

Figure 8. Latitude of Mars in the Martian moons' principal axis coordinate system, upper panel for Phobos, lower panel for Deimos.

simple model, and these values are an order of magnitude smaller than the longitudinal librations.

4.4. Consideration of Two Minor Perturbations

With the fitted initial conditions, we test here the two perturbations that were not introduced in the newly established dynamical model. An easy way to quantify them is to perform the difference between a first simulation involving the perturbation and a second simulation without them. The differences between one simulation with and one simulation without each perturbation tested are integrated over 10 yr and presented in Figures 9–11. The first perturbation tested here is the influence of the three largest asteroids, 1 Ceres, 2 Pallas, and 4 Vesta. Their orbit informations are taken from the JPL SPICE kernel files (https://naif.jpl.nasa.gov/pub/naif/). The simulations indicate that this perturbation introduces only several centimeters of influence on the satellites' orbit, and the effect on rotation is also very small, less than 0.2 milliarcsecond.

The second perturbation that has been tested is the presence of the mutual mass torques between the two Martian moons. For example, the point torque from Deimos to Phobos' figure can be calculated by

$$\boldsymbol{T}_{\mathrm{figP-pmD}} = \boldsymbol{f}_{\mathrm{figP-pmD}} \times (\boldsymbol{r}_{\mathbf{p}} - \boldsymbol{r}_{\mathbf{d}}), \tag{17}$$

where $\boldsymbol{f}_{\mathrm{figP-pmD}}$ is the force acting on Deimos as a point mass in Phobos' gravitational field, and in turn one can calculate the torque of the point mass Phobos on Deimos. The main related effect is that the torque on Deimos from Phobos' point

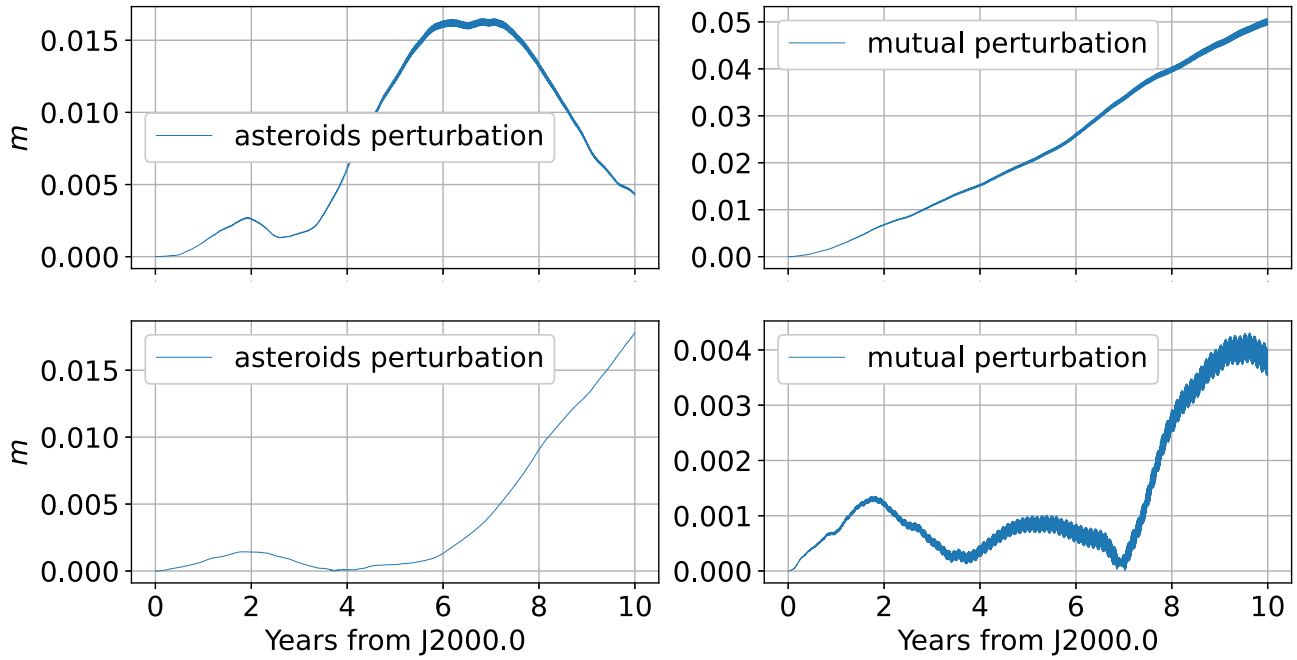

Figure 9. Orbital differences with and without asteroid perturbations and mutual perturbations. The perturbations tested here are the three largest asteroids acting on Phobos (upper left panel) and Deimos (lower left panel), and the mutual point mass torques on Phobos (upper right panel) and Deimos (lower right panel).

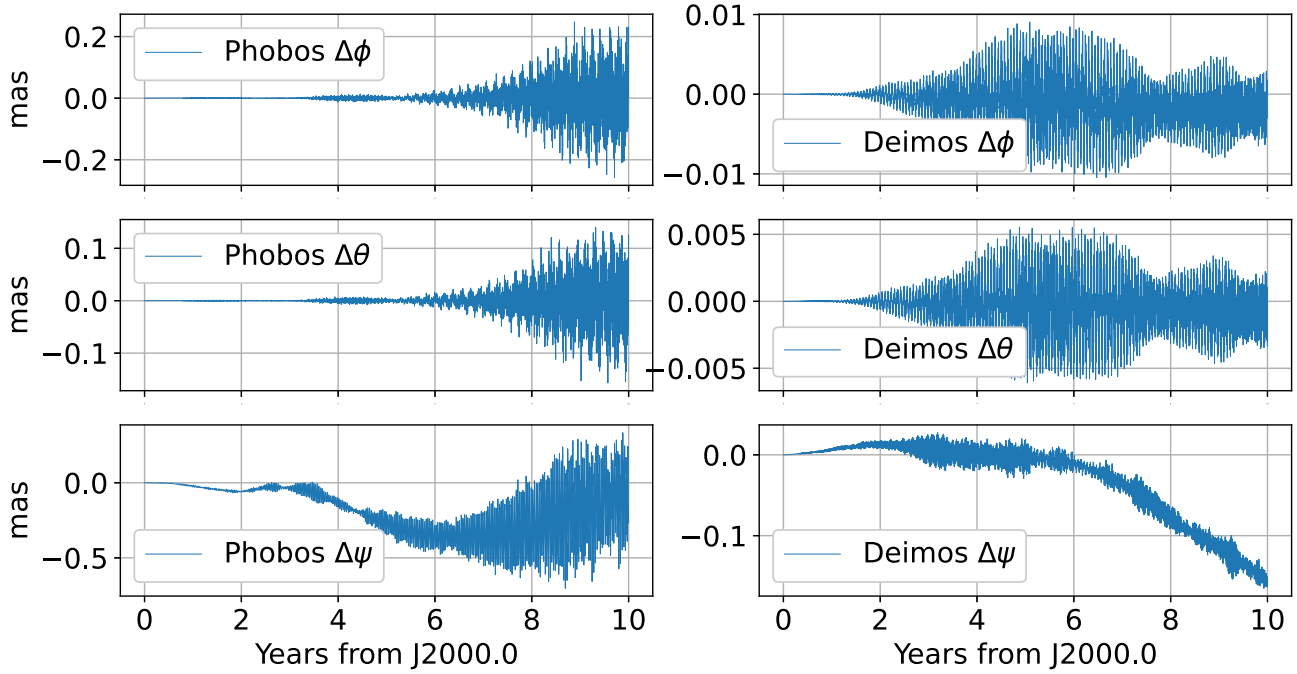

Figure 10. Euler angle differences between two cases involving asteroids' perturbations or not, left panels are for Phobos and right ones are for Deimos.

mass can lead to the difference in rotation angle reaching up to 1″ over 10 yr. The results show that none of the two perturbations considered in this section appear to have an effect on the orbit at an observable level. For the rotation, the effect of the point mass torque by Phobos on Deimos' rotation can reach up to 1 arcsecond, so this factor is recommended to be taken into account in the modeling process.

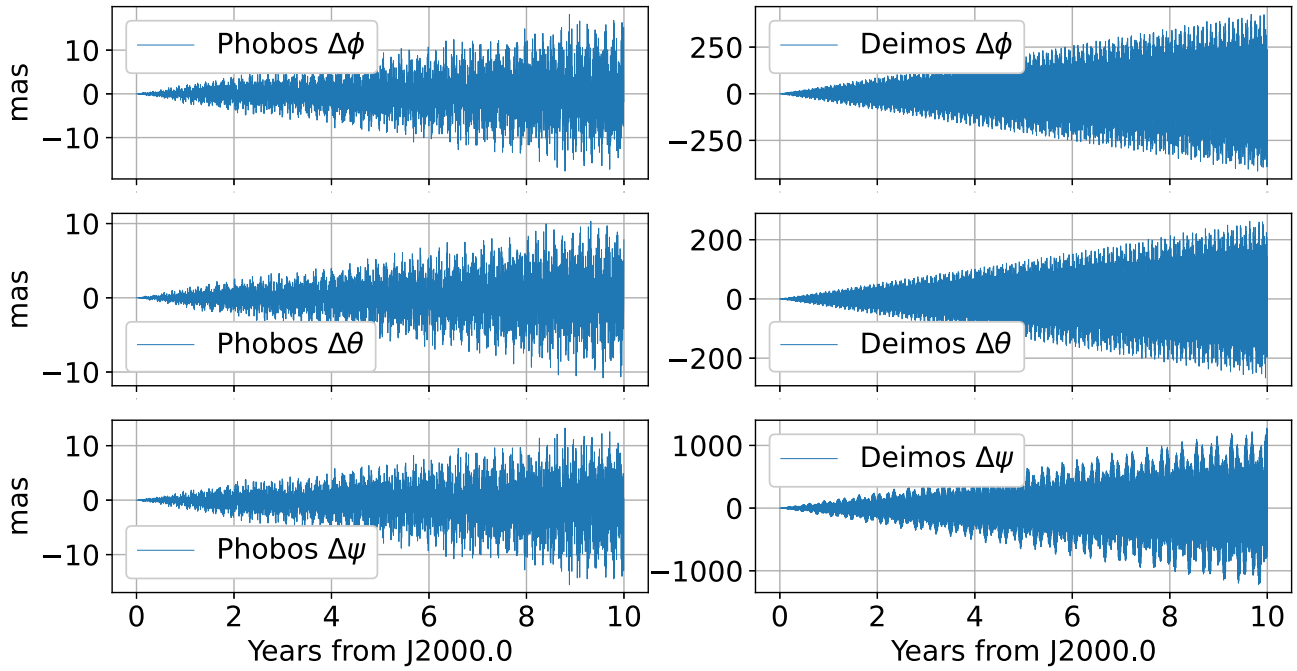

Figure 11. Euler angle differences between two cases involving mutual point mass torque or not, left panels are for Phobos and right ones are for Deimos.

5. Conclusion

High-precision numerical ephemerides typically provide information on the position, velocity and orientation parameters of celestial bodies over time, in addition to allowing detailed studies of the evolution and internal structure of those bodies. This work developed a new numerical dynamical model of the motions of the Martian satellites, taking full account of their rotation, and constructed a dynamical model of the coupled orbits and rotations using a method often applied in the study of the motion of the Moon (Folkner et al. 2014; Pavlov et al. 2016). In order to study the differences between the newly developed model and the dynamical model now in use, we first reproduced the ephemerides model, which was fitted to the ephemerides NOE-4-2020 published by Paris Observatory (Lainey et al. 2020) with the least-squares method, and then used it as the reference for which the newly developed model was fitted. The differences between the post-fit orbits of Phobos and Deimos for the two models are no more than 300 m and 125 m, respectively.

For the first time, we have computed simultaneously the Euler angles and their rates for Phobos and Deimos by numerical integration (Rambaux et al. 2012), and confirmed that the results are in good agreement with IAU values. Moreover, we simulated two possible perturbations which were not adopted in our refined model, and find that their effects on the orbits are completely negligible. As for the effect on rotation, we propose to consider the role of mutual attraction on rotation.

This revised numerical model of the motion of the Martian satellites provides potential opportunities for further study of the Martian satellites using high-precision observations from future missions such as MMX. In the future, not only the positions but also orientation parameters of the satellites can be derived from the refined dynamical model (Yang et al. 2024). Finally, our improved model of the dynamics of the Martian satellites employs a generalized approach that can be extended to systems beyond the Martian system, such as Saturn and Jupiter, by appropriately treating the rotational model.

Acknowledgments

This research was supported by the National Key Research and Development Program of China (2021YFA0715101), the National Natural Science Foundation of China (NSFC, grant Nos. 12033009 and 12103087), the Strategic Priority Research Program of the Chinese Academy of Sciences (XDA0350300), the International Partnership Program of Chinese Academy of Sciences (020GJHZ2022034FN), the Yunnan Fundamental Research Projects (202201AU070225, 202301AT070328, 202401AT070141), and the Young Talent Project of Yunnan Revitalization Talent Support Program. We thank the two anonymous referees for their careful reviewing and nice suggestions that have been incorporated into and improved the paper. Y.-Z.Y. thanks Dr. Valéry Lainey for his valuable suggestions which helped to improve the paper, and thanks Dr. Qingbao He for his help on spectrum analysis. Martian moons' ephemerides files can be found at ftp://ftp.imcce.fr/pub/ephem/NOE/(NOE-4-2020).

ORCID iDs

Yong-Zhang Yang https://orcid.org/0000-0001-9202-7750
Jian-Guo Yan https://orcid.org/0000-0003-2612-4776

References

Archinal, B., Acton, C., A'Hearn, M., et al. 2018, CeMDA, 130, 22
Arora, N., & Russell, R. P. 2010, CeMDA, 108, 107
Chao, B. F., & Rubincam, D. P. 1989, GeoRL, 16, 859
Fienga, A., Deram, P., Viswanathan, V., et al. 2020, in Proc. of the Journées 2019 "Astrometry, Earth Rotation, and Reference Systems in the GAIA era", ed. C. Bizouard, 293
Fienga, A., Deram, P., Di Ruscio, A., et al. 2021, NSTIM, S#110, 19
Folkner, W. M., Williams, J. G., Boggs, D. H., Park, R. S., & Kuchynka, P. 2014, IPNPR, 196, 1
Goldstein, H., Poole, C., & Safko, J. 2002, Classical Mechanics (San Francisco, CA: Addison-Wesley)
Jacobson, R. 2010, AJ, 139, 668
Jacobson, R., & Lainey, V. 2014, P&SS, 102, 35
Jacobson, R., Synnott, S., & Campbell, J. 1989, A&A, 225, 548
Kawakatsu, Y., Kuramoto, K., Ogawa, N., et al. 2017, in Proc. of International Astronautical Congress: : Unlocking Imagination, Fostering Innovation and Strengthening Security (Paris: IAF), 2732
Kawakatsu, Y., Kuramoto, K., Usui, T., et al. 2023, AcAau, 202, 715
Konopliv, A. S., Asmar, S. W., Folkner, W. M., et al. 2011, Icar, 211, 401
Konopliv, A. S., Park, R. S., Rivoldini, A., et al. 2020, GeoRL, 47, e2020GL090568
Konopliv, A. S., Yoder, C. F., Standish, E. M., Yuan, D.-N., & Sjogren, W. L. 2006, Icar, 182, 23
Lainey, V., Dehant, V., & Pätzold, M. 2007, A&A, 465, 1075
Lainey, V., Pasewaldt, A., Robert, V., et al. 2020, A&A, 650, A64
Le Maistre, S., Rosenblatt, P., Rambaux, N., et al. 2013, P&SS, 85, 106
Pätzold, M., Andert, T., Tyler, G., et al. 2014, Icar, 229, 92
Pavlov, D. A., Williams, J. G., & Suvorkin, V. V. 2016, CeMDA, 126, 61
Pitjeva, E., & Pavlov, D. 2017, EPM2017 and EPM2017H, Institute of Applied Astronomy RAS
Rambaux, N., Castillo-Rogez, J., Le Maistre, S., & Rosenblatt, P. 2012, A&A, 548, A14
Rubincam, D. P., Chao, B. F., & Thomas, P. C. 1995, Icar, 114, 63
Sharpless, B. P. 1945, AJ, 51, 185
Shor, V. A. 1975, CeMec, 12, 61
Sinclair, A. 1971, MNRAS, 155, 249
Sinclair, A. 1978, VA, 22, 133
Sinclair, A. 1989, A&A, 220, 321
Usui, T., Kuramoto, K., & Kawakatsu, Y. 2018, in 42nd COSPAR Scientific Assembly, B4.2–7–18
Viswanathan, V., Fienga, A., Gastineau, M., & Laskar, J. 2017, NSTIM, #108, 39
Williams, J. G., Boggs, D. H., Yoder, C. F., Ratcliff, J. T., & Dickey, J. O. 2001, JGR, 106, 27933
Willner, K., Shi, X., & Oberst, J. 2014, P&SS, 102, 51
Yang, Y., He, Q., Ping, J., Yan, J., & Zhang, W. 2019, Ap&SS, 364, 218
Yang, Y., Yan, J., Guo, X., He, Q., & Barriot, J.-P. 2020, A&A, 636, A27
Yang, Y., Yan, J., Jian, N., Matsumoto, K., & Barriot, J. 2024, A&A, 685, A13
Yang, Y.-Z., Li, J.-L., Ping, J.-S., & Hanada, H. 2017, RAA, 17, 127